Hindawi
Geofluids
Volume 2020, Article ID 8897911, 16 pages
https://doi.org/10.1155/2020/8897911

Research Article

Experimental Investigation on the Stress-Dependent Permeability of Intact and Fractured Shale

Yongxiang Zheng,[1,2] **Jianjun Liu**,[2,3] **Yichen Liu**,[2,4] **Di Shi**,[2,3] **and Bohu Zhang**[2]

[1]*School of Civil Engineering, Shijiazhuang Tiedao University, Shijiazhuang, China*
[2]*School of Geoscience and Technology, Southwest Petroleum University, Chengdu, China*
[3]*Institute of Rock and Soil Mechanics, Chinese Academy of Science, Wuhan, China*
[4]*Team 141 of Sichuan Coalfield Geological Bureau, Deyang, China*

Correspondence should be addressed to Jianjun Liu; jjliu@whrsm.ac.cn

Received 3 March 2020; Revised 29 July 2020; Accepted 21 August 2020; Published 10 September 2020

Academic Editor: Qian Yin

Copyright © 2020 Yongxiang Zheng et al. This is an open access article distributed under the Creative Commons Attribution License, which permits unrestricted use, distribution, and reproduction in any medium, provided the original work is properly cited.

The permeability of shale is extremely low. Therefore, the shale reservoir needs fracturing. The fracture network by fracturing can increase the permeability in a stimulated shale reservoir. To understand the permeability evolution in the stimulated shale reservoir, this study measured the permeability of intact and fractured shale samples with different pore pressure and confining pressure by the transient pulse test. And the differences between the two kinds of samples in permeability were analyzed. The results show that permeability magnitude of fractured shale is increased by 5 orders compared to the intact shale. It means that fracture networks after fracturing can effectively improve the permeability. Besides, the change in matrix permeability is the result of the combined effect of slippage effect and matrix deformation. At low pore pressure, the influence of slippage effect is more significant. Based on the results, an improved exponential function was established to describe the relationship between permeability and effective stress of shale matrix. Moreover, the permeability of fractured shale is still bigger than that of the shale matrix when the confining pressure is larger than pore pressure. This paper provides theoretical guidance for studying the evolution of reservoir permeability before and after fracturing.

1. Introduction

Low permeability and porosity of shale cause difficulties in shale gas exploitation [1]. Fortunately, combined with the complex structure of deep underground formation [2], the reservoir can be stimulated by hydraulic fracturing. Hydraulic fracturing is an effective method for shale gas exploitation. Fracturing is designed to create fracture networks by producing more fractures. The flow paths of gas in the stimulated shale reservoir include shale matrix and fracture network [3, 4]. It is difficult to flow in matrix with low permeability. Therefore, fractures are the main flow paths for shale gas.

Firstly, the permeability of matrix is affected by stress and flow regimes [5, 6]. Previous studies indicated that permeability is affected by the stress condition of shale reservoir. The stress of formation is affected by underground resource development [7, 8]. With the exploitation of shale gas, the reservoir pressure decreases and the effective stress increases, which will lead to the deformation of the shale matrix and the change of reservoir permeability [9]. Stress sensitivity is defined to describe the effect of pore-throat shrinkage on permeability [10]. Therefore, understanding the relationship between permeability and stress in shale reservoir can provide guidance for effective exploitation of shale gas. In addition, permeability of matrix is also affected by the porosity of the matrix. Due to the small porosity of the matrix, the slippage effect of gas in the matrix is significant at low pressure [5].

The stress sensitivity is the effect of pore-throat shrinkage on permeability. The pore-throat shrinkage is the result of effective stress change. Therefore, the effective stress is a vital factor on shale permeability. There are many studies on permeability and effective stress. The relationship between them can be described by exponential, logarithmic, and power

relationships [11]. Based on the laboratory experiment, Dong et al. [12] adopted the power law to describe the relationship between permeability and effective stress. And some other scholars [13, 14] suggested that power functions are appropriate to describe this relationship. There are also some studies that applied the logarithmic relationship to describe the stress sensitivity of permeability. Jones [15] described fractured carbonate permeability with respect to effective stress by a logarithmic empirical relationship. Walsh [16] represented the theoretical derivation procedure of this logarithmic relationship by using Poiseuille's equation of fracture system. Among them, the most popular empirical relationship is the exponential relationship. Zhang et al. [17] measured the permeability of shale in Lower Silurian Longmaxi Formation and suggested that the exponential law can well describe the relationship between shale permeability and various effective stress. Other studies [18–20] about shale permeability also showed that the exponential law was an appropriate method to present the relationship. In conclusion, the exponential relationship is the most widely accepted. Therefore, exponential function was chosen as the basic relationship to describe permeability and effective stress.

The fractures are the main flow path. Therefore, permeability considering fractures is of great importance to shale reservoir. There are some laboratory or theoretical studies about permeability of fractured shale. Wu et al. [21] and Tan et al. [22] studied the permeability evolution of proppant-supported fractures under dynamic stress conditions by a series of laboratory experiments. Generally, the cracks in fractured shale were created by artificial splitting. Besides, some splitting fractures were generated after high-temperature exposure in Yin et al.'s experiment [23]. Based on the fractured cores, Su et al. [24] studied the effect of mechanical opening (normal displacement) of fractures on the permeability. Zhou et al. [25] indicated that the fracture permeability was mainly determined by several factors including the shear displacement, integral roughness of the fracture planes, and the local roughness. Ma et al. [26] investigated the anisotropic permeability of cubic samples from Lower Silurian Longmaxi Formation. The results suggested that microfractures were critical to permeability in the parallel to bedding direction. And Zhou et al. [27] investigated the permeability change in a stimulated shale gas reservoir under high effective stress. Then, they derived a stress-dependent fracture permeability model based on the fracture compressibility models. Yin et al. [28] conducted stress-dependent flow tests on real rock specimens containing fracture networks with various included angles. Chen et al. [29] derived a theoretical correlation between shale permeability and effective stress. The results indicated that fracture permeability might decrease significantly with the reservoir pressure drawdown.

There are some meaningful results about the permeability of shale in previous studies. However, the researches on the stress sensitivity of shale matrix were mainly based on the research with high pore pressure, and less consideration was given to the permeability variation rule with low pore pressure. In this study, the permeability of intact shale (shale matrix) and fractured shale as a function of pressure was measured. For the permeability of shale matrix, we measured the stress sensitivity of permeability under both low and high pore pressures. In addition, we improved the exponential model to characterize the permeability and effective stress of shale matrix. By comparing the new model with the experimental results and the experimental data in the existing literature, it is found that the improved exponential relation has a higher fitting accuracy. For fractured shale, we analyze the permeability evolution law of fractured shale and discuss the reason why stimulated new fractures can still increase reservoir permeability after closure. In addition, equivalent fracture width is applied to characterize the permeability of fractures, and the relationship between equivalent fracture width and effective stress is established. The results include the permeability evolution of shale matrix and fracture system, which provides a theoretical basis for the permeability evolution of stimulated reservoir in the process of shale gas development.

The innovation of this article is mainly reflected in the following three aspects. The first innovation of this article is to supplement and improve the experimental plan. The experiment tests the permeability changes under low pore pressure and high pore pressure conditions and discusses the effect of slippage effect and effective stress on permeability. Most of the previous people only considered the effect of effective stress under high pore pressure conditions. In addition, this experiment also measured the permeability of fractured shale and intact shale and analyzed the influence of fracture on the overall permeability of shale sample by comparison. The second innovation is the improvement of the traditional exponential relationship. The fitting results of the experimental results in this experiment and other literatures indicate that the improved relationship has higher fitting accuracy. The third innovation is to analyze the reason why the permeability of the fracture after the fracturing is still higher than that of the matrix when the confining pressure is greater than the pore pressure.

2. Materials and Methods

2.1. Introduction of Samples. The samples were taken from the Longmaxi Formation in the Changning section of Shuanghe Town, Sichuan Basin. The sampling site is located in Yanzi Village, Shuanghe Town, Yibin City, Sichuan Province, China. The Silurian Longmaxi Formation is composed of black, gray-black, and dark gray calcareous and siliceous shale and sandy shale. And it is in integrated contact with the underlying Upper Ordovician.

The uniaxial compression test and SEM test were chosen to determine the mechanical properties and microstructure of the samples. The uniaxial compression test showed that the elastic modulus was in the range of 14.04-25.69 GPa and the Poisson's ratio was in the range of 0.14-0.389. The results indicated that the samples were hard to deform with a higher elastic modulus. Elastic modulus is a measure of the ability of an object to resist elastic deformation. Then, the greater the elastic modulus, the greater the object's ability to resist elastic deformation. Under a certain load, the greater the elastic modulus, the smaller the deformation.

Figure 1: The microscopic pore of shale samples.

The SEM test has an ultrahigh resolution and can produce secondary electron images of the surface appearance of various solid specimens and comprehensively analyzes the surface characteristics of rocks [30, 31]. The SEM test was employed to understand the microscopic pore structure of shale samples. The results are shown in Figure 1. Figure 1(a) is a SEM photo of the shale surface magnified 1000 times. The figure shows that the voids mainly include microfractures and pores. The main of void volume on the surface is micropores. To show the micropores more clearly, the local micropores (yellow rectangle in Figure 1) were enlarged. Figure 1(b) shows the SEM photo magnified 5000 times. In the figure, the reference scale is 40 μm. As can be seen from the figure, the pore size is significantly smaller than the scale length. Therefore, the scale of micropores in the matrix is in nanoscale. In addition to micropores, there are some scattered fractures on the surface. The fracture area is amplified locally to observe the morphology of those fractures. Figures 1(c)–1(e) show the morphology of the three microfractures, respectively. As shown in the figures, the fracture length is much larger than the radius of micropores. The micropores are connected by those long fractures. As the microstructure of matrix shows, the scale of pore in matrix is very small. The small pores result in the low permeability. Besides, there are some fractures. However, the fractures are not long enough to connect with other fractures. Therefore, the permeability of matrix is still low. To some extent, it can be considered that few microfractures do not increase permeability.

2.2. Sample Preparation. The main purpose is to study the permeability variation of the intact and fractured shale. As shown in Figure 2, there are 4 cylindrical samples with a diameter of 25 mm and a height of 50 mm drilled from the outcrop. Among them, KJ1 and KJ2 are intact cores without fractures. KJ3 and KJ4 are fractured cores with artificial fractures. A schematic view of the fractured core is shown in Figure 2(b). As shown in the figure, a fracture located approximately in the middle of core penetrates this core. An end surface is shown in Figure 2(c). To obtain accurate experimental results, the geometry, weight, and porosity of each core were measured. The details are listed in Table 1.

From Table 1, the porosity range of the shale matrix falls in the range from 4.08% to 4.71%, while the porosity range of the fractured cores is from 6.77% to 7.01%. The porosity of each sample is at a low scale overall. Besides, the porosity of the fractured core is slightly bigger than that of the intact core. This indicated that fractures increased the porosity of the samples.

2.3. Laboratory Measurement System. The Black-Stone II stress-sensitive pulse tester, which was jointly developed by the Institute of Rock and Soil Mechanics of the Chinese Academy of Sciences and Southwest Petroleum University, was chosen to measure the permeability. The photo of this device is shown in Figure 3(a). And this device measures permeability by the transient pulse method. This test system mainly includes a confining system, upstream system, downstream system, and core holder. The details are plotted in Figure 3(b). The confining pressure (CP) of the system can be up to 60 MPa, and the pore pressure (PP) can be up to 40 MPa.

This device measures permeability by the transient pulse method. First, the pressure within the system should be balanced. Once the pressure is balanced, a transient pulse is applied to the upstream chamber (V1, Figure 3). Then, the pressure in V1 will gradually transfer to downstream chamber V2. Consequently, the pressure in V1 decreases, and the pressure in V2 increases until reaching a new pressure balance. A pressure decay curve at V1 can be plotted during

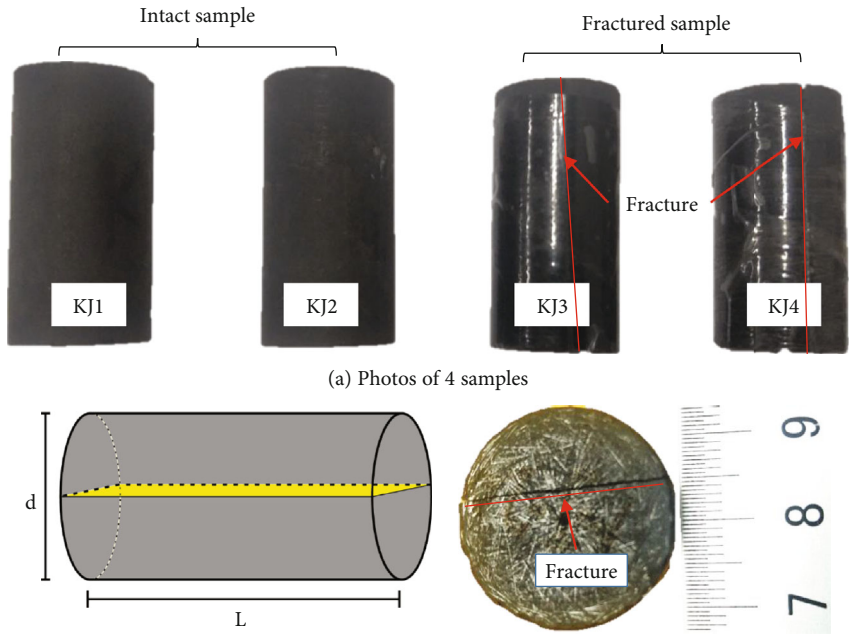

(a) Photos of 4 samples

(b) Schematic diagram of the fractured sample

(c) End surface of the fractured sample

Figure 2: The intact and fractured samples.

Table 1: The parameter values of samples.

No.	Length (cm)	Diameter (cm)	Weight (g)	Porosity
KJ1	4.998	2.535	63.87	4.08%
KJ2	4.987	2.536	63.56	4.71%
KJ3	5.025	2.418	56.65	7.01%
KJ4	5.011	2.422	57.27	6.77%

the pressure change. Based on this curve, the permeability of the test sample can be obtained. The mathematical model of permeability by the transient pulse method is [32, 33]

$$\frac{\partial^2 p}{\partial l^2} = \left[\frac{\mu}{k}\phi\left(C_f + \frac{C_{\text{eff}}}{\phi} - \frac{1+\phi}{\phi}C_s\right)\right]\frac{\partial p}{\partial t}, \quad t > 0, 0 < l < L, \tag{1}$$

where p is the pressure (MPa), l is the distance along the length of the measured rock sample (cm), k is the permeability of the measured rock sample (μm^2), μ is the dynamic viscosity of the fluid (10^{-3} Pa·s), φ is the porosity, C_f is the compression coefficient of the fluid (MPa^{-1}), C_s is the compression coefficient of samples (MPa^{-1}), and C_{eff} is the pore compression coefficient samples (MPa^{-1}). The boundary condition is

$$\begin{aligned} \frac{\partial p}{\partial l} &= \frac{\mu V_u C_f}{kA}\frac{\partial p}{\partial t}, \quad t > 0, l = 0, \\ \frac{\partial p}{\partial l} &= -\frac{\mu V_d C_f}{kA}\frac{\partial p}{\partial t}, \quad t > 0, l = L, \end{aligned} \tag{2}$$

where A is the cross-section area (cm^2), V_u is the volume of upstream chamber (cm^3), and V_d is the volume of downstream chamber (cm^3). The initial condition is

$$\begin{aligned} p_u(0,0) &= p_i \quad t = 0, l = 0, \\ p_R(l,0) &= p_0, \quad t = 0, 0 < l < L, \\ p_d(L,0) &= p_0, \quad t = 0, l = L, \end{aligned} \tag{3}$$

where p_i is the pressure of upstream chamber when the pulse pressure is applied (MPa).

The mathematical models of the transient pulse method mainly include an approximation method, plate method, and Jones' method. Due to the fact that the medium in this experiment was nitrogen, Jones' method was chosen for this test [34]. Jones' method is a simplification of a mathematical model for the transient pulse method. The analytical solution of the gas permeability can be expressed as

$$k_g = \frac{-14696 m_1 \mu_g L f_z}{f_1 A p_m((1/V_u) + (1/V_d))}, \tag{4}$$

where m_1 is the slope of the pressure decay curve, μ_g is the viscosity (10^{-3} Pa·s), f_z is the correction factor of gas compression, f_1 is the correction factor of mass flow, and p_m is the average pore pressure (MPa).

2.4. Experimental Testing Process and Design. Transient pulse testing of shale permeability can be divided into two parts: aging test and measurement. The aging test plays a crucial role in the measurement of stress sensitivity of permeability. The aging test eliminates irreversible deformation in the test by the loading and unloading process of the confining

(a) Photo of Black-Stone II pulse tester

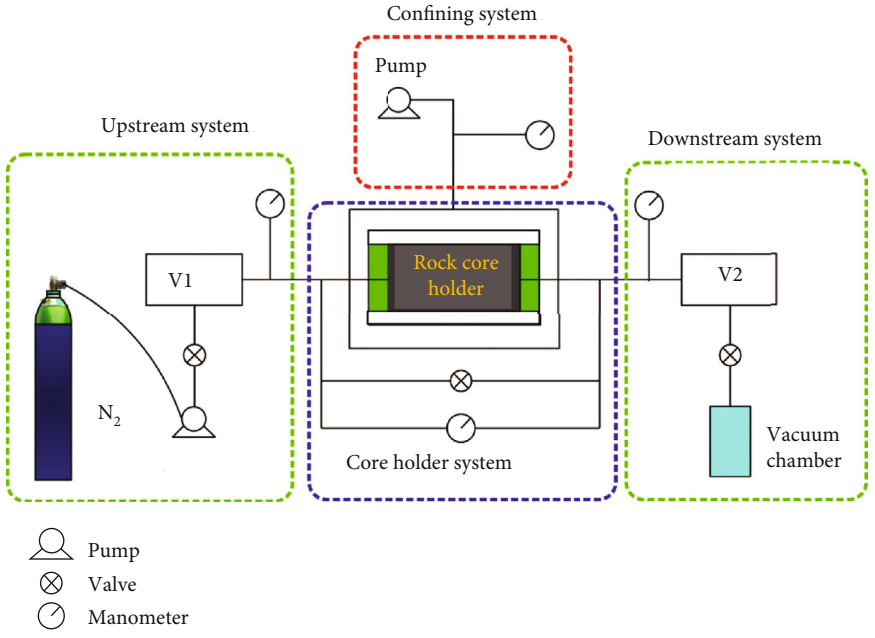

(b) Equipment composition diagram

FIGURE 3: The measurement system.

pressure. Therefore, the rock samples were first subjected to the aging test. Through the aging test, the stability and reliability of the test results can be improved. The steps of the aging test are as follows. First, the pore pressure and the chamber pressure should be stabilized. And the pore pressure is maintained at 0.8 MPa. Then, the confining pressure was sequentially increased from 5 MPa to 40 MPa with a step of 5 MPa. Next, the confining pressure is reduced from 40 MPa to 5 MPa with every step of 5 MPa. When the confining pressure is stabilized for every step, a pulse pressure is applied to determine the corresponding permeability. Repeat the loading-unloading pressure process.

After the aging test was completed, the permeability of sample can be measured. At first, the permeability changed by the pore pressure with a fixed confining pressure of 30 MPa was measured. The measured results are plotted in Figure 4. The permeability declines first and then rises with the increase of pore pressure. As the figure shows, the pore pressure at turning point is 6 MPa. According to the literature [5], the slippage effect in the matrix is obvious with low pore pressure. The slippage effect can increase gas permeability. The slippage effect becomes weaker as the pore pressure rises. Therefore, the permeability drops as the pore pressure rises. The slippage effect only occurs in the shale

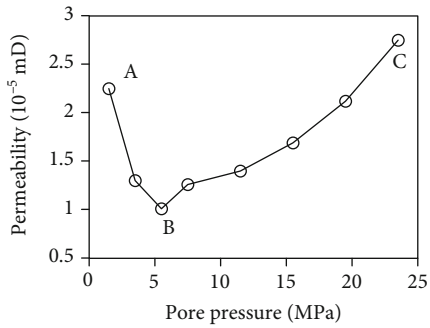

Figure 4: Relationship of permeability and pore pressure.

matrix, while the gas is in laminar flow in the fracture system. Therefore, this experiment discusses both low pore pressure (2-6 MPa) and high pore pressure (8-24 MPa) for intact shale. In addition, to analyze the permeability evolution of fractured shale, a permeability test scheme for fractured shale was designed. The details about experiments design are summarized in Table 2.

3. Results

3.1. Permeability of Intact Shale. Figure 4 shows the permeability curve of KJ1 changing with pore pressure at a fixed confining pressure of 30 MPa. As pore pressure rises, permeability drops first and then rises. When the pore pressure is less than 6 MPa, permeability reduces as the pore pressure rises. Qian et al. [35] and Yang et al. [5] also had the similar results by experiments. They believed that the effective stress decreased with the increase of pore pressure and then the matrix pores were larger. Consequently, the permeability of matrix is affected by both matrix deformation and slippage effects. In a low pore pressure (0-6 MPa), the slippage effect of gas is obvious, and its influence on the permeability is large. When the pore pressure is bigger than 6 MPa, the matrix deformation becomes the main factor. In this condition, the permeability increases with the increase of pore pressure.

In most cases, a pore with a large radius means large permeability. But a pore with a small radius may have a larger flow capacity than that with a large radius with a little difference in pore structure due to the slippage effect. The pore radius of the shale is too small to ignore the slippage effect due to low pore pressure. And the slippage effect is the main factor affecting permeability. Therefore, pores with a small radius have larger flow capacity. Conversely, when pores are larger, the slippage effect can be ignored. Matrix deformation becomes the main factor affecting permeability. Then, the large pore radius means large permeability.

In short, the slippage effect of gas on permeability is dominant when pore pressure is small. And permeability decreases as pore pressure rises. When pore pressure is larger than the critical pressure (6 MPa in this study), the key factor affecting permeability is matrix deformation. And permeability increases as pore pressure rises. It is worth noting that regardless of the low or high pore pressure, the permeability of matrix is affected by both slippage effect and matrix deformation. One factor will be the dominant factor under a certain condition. As mentioned above, the change of permeability with pore pressure is different under different pressure conditions. Therefore, the test about matrix permeability is divided into two cases: low pore pressure and high pore pressure.

3.1.1. Permeability Variation under Low Pore Pressure. Permeability variation under low pore pressure is discussed in this section. The matrix permeability is measured by changing confining pressure (abbreviated as CP in the next figures) with a fixed pore pressure (abbreviated as PP in the next figures). Figure 5(a) shows the results of permeability change with confining pressure when the pore pressure is 2, 4, and 6 MPa, respectively. First of all, it can be clarified that permeability decreases as confining pressure rises under a constant pore pressure. Besides, the decaying rate of permeability is faster at a low confining pressure. With the increase of confining pressure, it is more difficult for the shale matrix to be compressed. Consequently, the decaying rate of permeability reduces significantly. In addition, for one fixed confining pressure, permeability decreases as pore pressure increases. Moreover, the decrease magnitude of permeability between 2 and 4 MPa is greater than that of the interval of 4-6 MPa. It indicates that the decay rate of the permeability reduces as the pore pressure rises. This is consistent with the results of the A-B interval in Figure 4.

Permeability variation with effective stress is shown in Figure 5(b). For a fixed pore pressure, permeability is negatively related to effective stress. Moreover, the permeability is different even though the effective stress is the same. It can be deduced that the pore pressure is the reason for the difference. Overall, the permeability at lower pore pressure is bigger. It indicates that the effective stress is not the key factor for permeability change at low pore pressure. The key factor should be the slippage effect. Consequently, the pore pressure condition cannot be ignored for the relationship between permeability and effective stress at low pore pressure.

Generally, the reservoir pressure is maintained at a higher condition during gas development. The low pore pressure condition always appears in the late development period. At this time, the permeability of matrix would rise gradually as the reservoir pressure gradually decreases. Therefore, this conclusion is mainly used to guide the development of gas reservoir in the late period.

3.1.2. Permeability Variation at High Pore Pressure. Generally, the reservoir pressure is maintained at a higher value. With the gas production, the pore pressure gradually decreases, while the in situ stress of formation does not change significantly. Therefore, the experimental scheme of changing pore pressure with fixed confining pressure was selected. The results are shown in Figure 6. The order of matrix permeability is $1e^{-5}$ mD. The matrix permeability varies from $1e^{-5}$ to $5e^{-5}$ mD. Matrix permeability increases as the pore pressure increases. The slope of the curves is larger for higher pore pressure, indicating that the permeability is greatly affected by the pore pressure. Conversely, the curve

Table 2: Design of experiments.

	Samples	Test type	Confining pressure (MPa)	Pore pressure (MPa)
Intact shale	KJ1	Basic case	30	2, 4, 6, 8, 10, 12, 14, 16, 18, 20
	KJ1	Low pore pressure	10, 15, 20, 25, 30	2, 4, 6
	KJ1, KJ2	High pore pressure	30, 35, 40	8, 12, 16, 20, 24
Fractured shale	KJ3, KJ4	High pore pressure	30, 35, 40	8, 12, 16, 20, 24

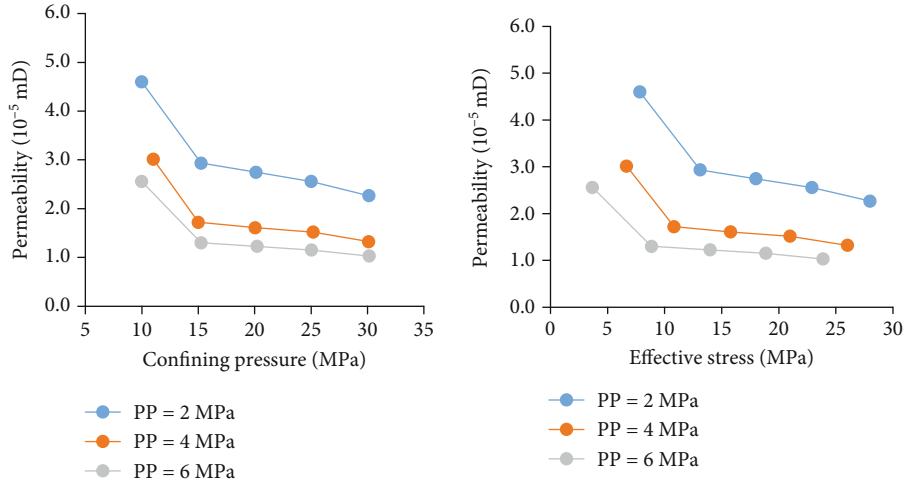

(a) Permeability vs. confining pressure (b) Permeability vs. effective stress

Figure 5: Matrix permeability at low pore pressure.

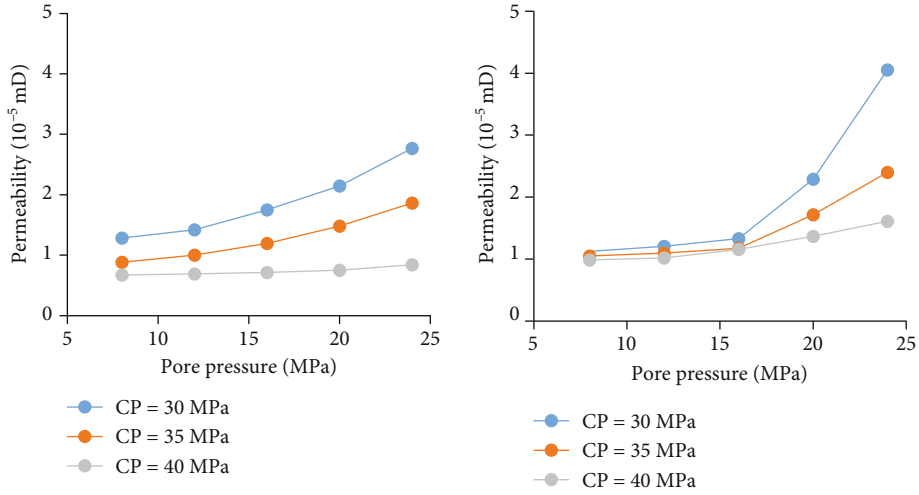

(a) Permeability of KJ1 (b) Permeability of KJ2

Figure 6: Relationship between permeability and pore pressure.

slope is smaller for lower pore pressure, indicating that the influence of pore pressure on the permeability reduces gradually. In the early period of development, the pore pressure is high. Consequently, the pore pressure has a great influence on the permeability during the early period. Then, the permeability gradually becomes stable in the late period of development when pore pressure reduces.

In addition, the permeability of matrix is also affected by confining pressure. As shown in the figures, the permeability varies greatly as pore pressure is 30 MPa. But the permeability varies little as pore pressure is 40 MPa. The confining pressure means a change in the depth of the reservoir. Therefore, the greater the depth of reservoir is, the less permeability of shale matrix is affected by pore pressure.

In short, the permeability of matrix is affected by both slippage effect and effective stress under different pore pressure and confining pressure. At the condition of low pore pressure, the permeability decreases with pore pressure increase, while at the condition of high pore pressure, the permeability rises with pore pressure increase. Besides, the

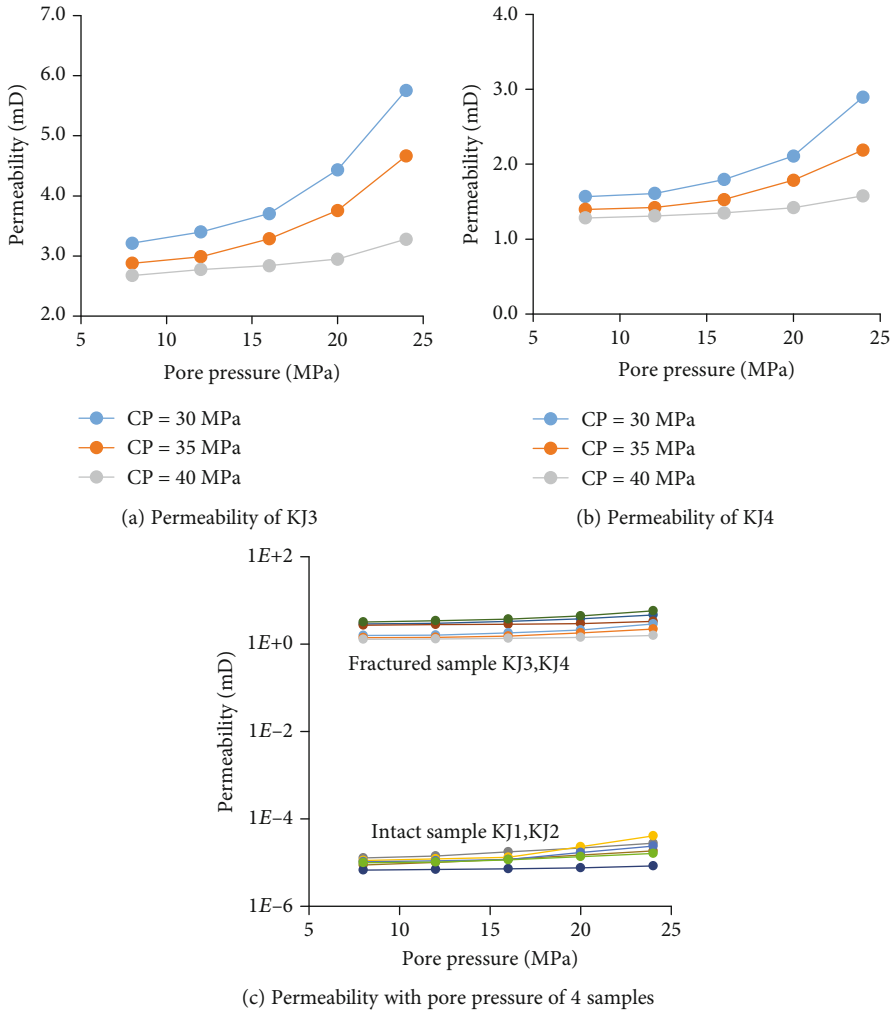

(a) Permeability of KJ3

(b) Permeability of KJ4

(c) Permeability with pore pressure of 4 samples

Figure 7: Relationship between permeability and pore pressure.

permeability of matrix reduces as confining pressure rises. The effect of gas slippage on permeability is significant at low pore pressure and weakened at high pore pressure.

3.2. Permeability of Fractured Shale. The permeability of fractured shale is discussed in this section. Figure 7 illustrates the influence of confining pressure and pore pressure on permeability of fractured shale. The permeability of fractured shale sample ranges from 1 mD to 6 mD. Permeability variation of fractured shale is similar to that of intact shale. The permeability rises as the pore pressure increases and reduces as the confining pressure increases.

The results of permeability for both intact and fractured shale are summarized in Figure 7(c). As the figure shows, permeability magnitude of fractured shale is raised by five orders compared to the intact shale. The fractures in this experiment do not contain proppants and can be considered self-supporting fractures. From the results above, we can safely draw a conclusion that the self-supporting fractures greatly enlarge the permeability of sample. And the fractures are the main flow paths for shale gas. For an ideal situation, if a fracture was completely closed by the confining pressure, there would no conductivity theoretically. Actually, the measured permeability is much bigger than the matrix permeability. This result is consistent with Gutierrez's conclusion: the fracture permeability remained much higher than the intact shale (or matrix) permeability [36]. Gutierrez just described the results but did not explain why. We would discuss the reason why the samples can still increase the permeability after the fractures closed in Section 4.2 as a discussion.

4. Discussion

4.1. Relationship between the Permeability of Matrix and Effective Stress

4.1.1. Improved Exponential Function. For the cases of high pore pressure, the permeability of matrix is mainly affected by matrix deformation. The main factor affecting matrix deformation is effective stress. Previous studies established some relationships to describe the influence of effective stress on matrix permeability. The exponential relationship is the

Table 3: The fitting results.

	Samples	$a(a_0)$	$b(b_0)$	$c(c_0)$	R^2
Traditional exponential function	KJ1	$3.918e-5$	0.04872	0.7157	0.9233
	KJ2	$4.031e-5$	0.04745	0.0.4336	0.8811
	(KJ1 + KJ2)/2	$4.744e-5$	0.05781	0.4081	0.9030
Improved exponential function	KJ1	$6.505e-5$	0.1356	$9.197e-6$	0.9540
	KJ2	$4.238e-5$	0.1006	$9.586e-6$	0.9007
	(KJ1 + KJ2)/2	$6.459e-5$	0.1415	$1.078e-5$	0.9769

most common approach. The traditional exponential function is shown in Equation (5). Based on the exponential relationship, this study improved traditional exponential function. The improved exponential relationship is shown in Equation (6).

$$k = a_0 e^{-b_0(\sigma_e - c_0)}, \tag{5}$$

$$k = a e^{-b\sigma_e} + c. \tag{6}$$

The results about the relationship between permeability and effective stress of samples KJ1 and KJ2 are listed in Table 3. Besides, the third set of experimental data was taken by the average of the two sets of data. Then, there are 3 sets of data. The traditional and improved relationship can be fitted, respectively, using these 3 sets of data by Matlab. The fitting is based on the Levenberg-Marquardt algorithm built into the software. The coefficients for the two relationships and the goodness of fit are shown in Table 3. The fitting results of the two relationships are shown in Figure 8.

As shown in Figure 8, permeability decreases as the effective stress rises. Different with the results of low pore pressure in Figure 5(b), the difference in permeability values for one effective stress value is small, indicating that the matrix deformation is the key factor affecting permeability at high pore pressure. We also focus on the slope of curves. The decaying rate of permeability is large when the effective stress is low. And as the effective stress rises, the decaying rate of permeability is gradually slowing down. It can be explained by the reason that the deformation of compacted rock is more difficult for higher effective stress.

It is generally believed that in situ stress in the reservoir remains stable. The reservoir pressure in the early period of development is high, and the effective stress is small consequently. In such a condition, the pressure change induced by gas extraction would have great impact on permeability. In the late period of development, the pore pressure reduces and the effective stress rises. In such a condition, the change of pore pressure has little effect on the overall permeability.

The fit goodness (R^2) is a mathematical index reflecting the effect of data fitting. As Table 3 shows, the fit goodness for the improved exponential function is 0.9540, 0.9007, and 0.9769. The R^2 of improved exponential function is higher than that of the traditional exponential function. The new function can better fit the relationship between permeability and effective stress.

In order to verify whether the model is suitable for other data, the improved function is applied to fit the results from other results. The fitted data is derived from the results of Duan et al.'s study [37]. The fitting results are shown in Figure 9. The red dots in the figure are the measured data points. The dashed lines are the fitting results by the traditional exponential function in Equation (5). The solid lines are the fitting result by the improved exponential function in Equation (6). As the figure shows, the fitting goodness of samples 209, 215, and 239 by the improved exponential function was 0.9988, 0.9966, and 0.9741, respectively. It means that the improved exponential function proposed in this paper is better than the traditional exponential function in fitting accuracy.

4.1.2. Parameter Analysis of the Three Coefficients in the Improved Exponential Function. Each coefficient of the improved exponential function has its own attributes. Compared with the traditional exponential function, there is a constant c in the new function. When the effective stress is zero, the permeability is $a + c$. And when the effective stress tends to infinity, the permeability is c. According to the traditional exponential relationship, a is the corresponding permeability when effective stress is zero. In addition, when the effective stress tends to infinity, the permeability should be zero. Actually, the permeability is not zero. Therefore, the fitting effect of the new model is better after adding a new constant c. The constant c can be understood as the deviation due to the experimental system or other factors. It can also be seen from the data in Table 3 that the value of the constant c is generally small compared to the value of a. However, the fitting effect of the experimental results after introducing the constant c is better.

The effect of each coefficient on the permeability curve is shown in Figure 10. The values of the three coefficient are selected according to the value in Table 3. In Table 3, the value of coefficient a is from $4.23e-5$ to $6.50e-5$. Therefore, $5e-5$ was set as the basic value. Then, the range was selected from $0.5e-4$ to $2.5e-4$. Figure 10(a) shows the effect of the constant a on the curve. According to the traditional exponential relationship, the constant a represents the corresponding permeability when the effective stress is zero. The initial permeability is defined as the corresponding permeability when the effective stress is 0. As the figure shows, the initial permeability rises as the value of a rises. The permeability curves with different constants a would converge when effective stress reaches 30 MPa.

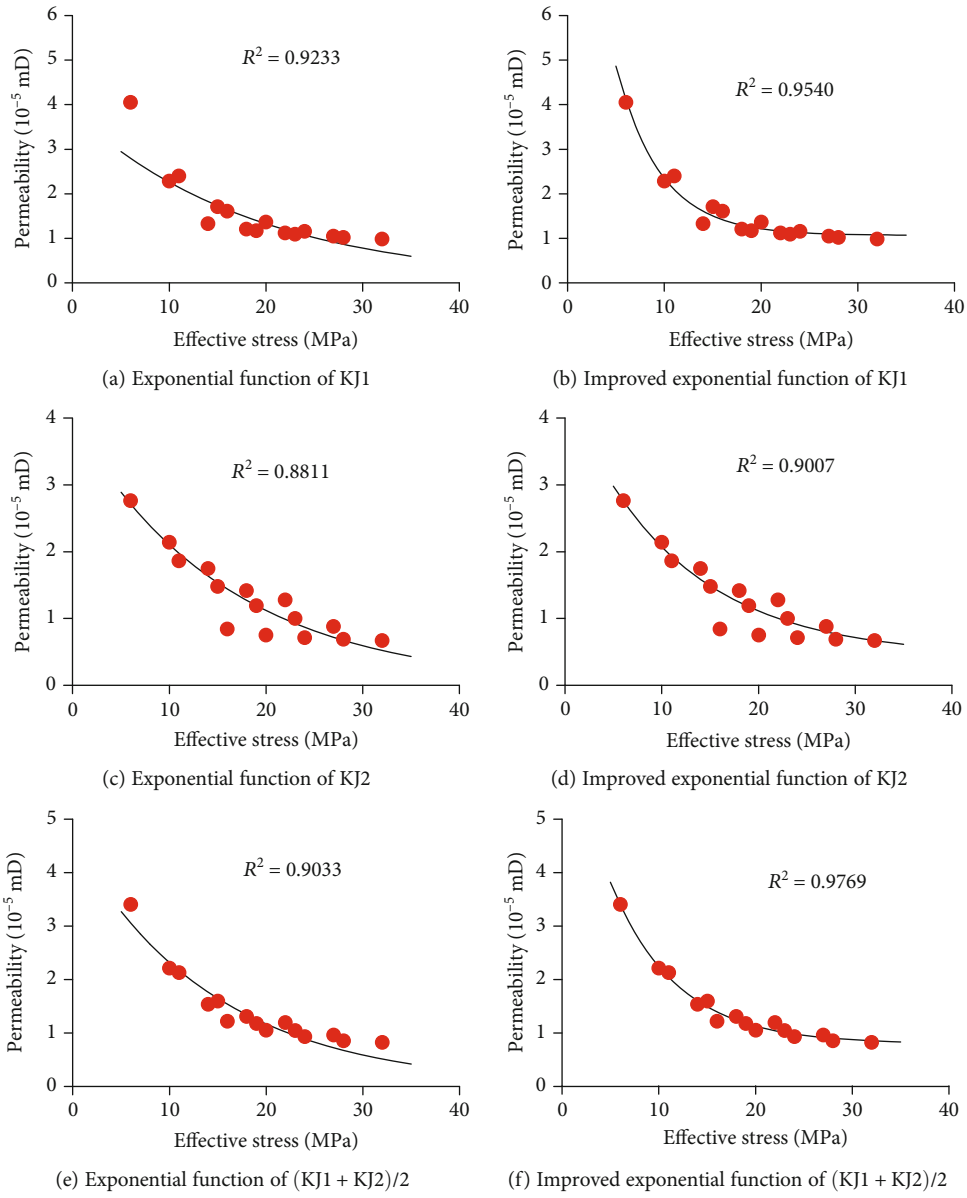

Figure 8: Fitting results of permeability with effective stress.

Figure 10(b) shows the effect of the coefficient b on the permeability curves. The coefficient b is considered the stress sensitivity coefficient. As shown in the figure, the influence of coefficient b on permeability is divided into two aspects. The first aspect is the effect on the decaying rate of permeability. The larger the coefficient b value is, the larger the decaying rate of the curve is. When b is equal to 0.1, the decay rate of the curve is small and the curve is gradual. As b rises, the curves become more curved. The second aspect is the sensitive range of effective stress. According to the curves, permeability is greatly affected by the effective stress with small effective stress, and the permeability gradually becomes stable with large effective stress. Therefore, the permeability sensitivity is very obvious within a certain range. It can be seen from the figure that the larger the b value is, the smaller the range where the permeability is significantly affected by the effective stress is. Then, the influence of the constant b on the permeability can be obtained. Naming the range where permeability is more significantly affected by the effective stress as sensitivity range. The sensitivity range decreases as the constant b increases.

Figure 10(c) shows the effect of the coefficient c on permeability curves. The curves only shift vertically as c changes, and the shape of the curves does not change. As mentioned above, the value of c is very small compared to the initial permeability a. This coefficient c can be considered the fluctuation of the permeability test caused by the experimental system or other reasons. The introduction of the coefficient c is more conducive to the fit of the relationship between permeability and effective stress, although c is small.

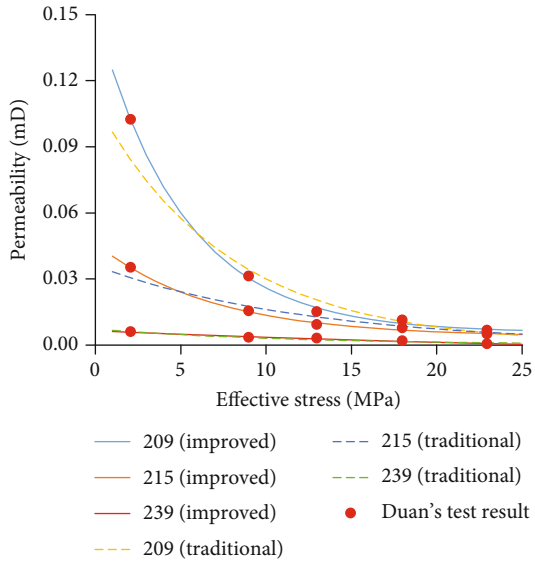

FIGURE 9: Model verification of the improved exponential relationship.

4.1.3. Comparison of Traditional and Improved Models. There are three advantages of the new model compared with the traditional model. Firstly, the new model can get better fitting accuracy. The new model is verified by the results of this experiment and a previous experiment. Both of these indicate that the fitting accuracy of the new model is better.

Secondly, although the expressions of the two models seem similar, there are differences in the mathematical form. Let $A = a_0 e^{b_0 c_0}$; then, the traditional model becomes

$$k = Ae^{-b_0\sigma_e} \quad \text{(traditional model)}. \tag{7}$$

The new model is

$$k = ae^{-b\sigma_e} + c \quad \text{(improved model)}. \tag{8}$$

Comparing the two models, the effect of the parameter c_0 in the traditional model is essentially on A. The parameter A is a multiplication factor, which will enlarge or reduce the entire curve. The parameter c is just a constant term. Therefore, the constant c can be more flexible in the fitting process and leads to the up and down translations of the curve. Consequently, the new model can have better fitting accuracy.

Third, as mentioned in the second point, the new model can express the up and down translations of the curve. Therefore, the new model can reflect the overall error caused by the equipment and measurement process. This can make the fitting result more accurate.

4.2. The Permeability of Self-Supporting Fractures

4.2.1. Conductivity of Self-Supporting Fractures. Fractures are the main flow channels of shale gas. Therefore, it is of great significance to understand the permeability variation induced by fractures. Generally, fractures can be divided into self-supporting fractures and supporting fractures depending on whether or not the proppants are contained. The self-supporting fractures without proppants were measured in this experiment. In this section, the permeability variation of self-supporting fractures would be discussed.

Although the self-supporting fracture closes apparently, it still plays a major role in permeability of the shale system. In an ideal state, fractures would be closed when confining pressure is greater than pore pressure. If a fracture is closed completely, the measured permeability should be the same with the permeability of the matrix. However, the actual measured permeability was much greater than the permeability of matrix. As shown in the results of this experiment, the fractures without proppants are still permeable when the confining pressure is larger than pore pressure. It indicates that the fractures are not closed completely. Therefore, the permeable fractures without proppants are called self-supporting fractures.

Ren et al. [31] shared the same idea that the fracture did not close completely. Then, why does the fracture cannot close completely? Self-supporting fractures without proppants are permeable. The profiles of the samples in Figure 11(a) show that fracture surfaces are of certain roughness. The fracture surfaces may be slightly distorted under stress conditions. A slight displacement between the fractures faces results in the incomplete contact between two fracture faces. Therefore, the small displacement between the rough fracture faces is one of the main reasons for the unclosed fractures. In the real stratum, the in situ stress conditions are complex, and the fracture surfaces are relatively dislocated under the action of shear stress after fracturing. As Yin et al.'s experiment about the influence of shear processes on nonlinear flow behavior through3D rough-walled rock fractures shows, the relative displacement of the rough surfaces under shearing would form a flow passage between the fractures [38]. The permeability of fractured shale is related to the roughness and relative shear displacement of the fracture surfaces.

In addition, another reason is the flaking of particles during the prefabrication of fractures. When the fracture was prefabricated, some of the blocks on the fracture surfaces peeled off. The blocks in our other related experiments about fracking are shown in Figure 11(b). The size and scale of the peeling block are different. Its size ranges from strip to powder. These blocks contribute to the permeability of self-supporting fractures in two ways. First, there will be gaps between the surfaces which are the flow channels for gas after block peeling off. It increases the permeability of the rock sample, which may also be a reason for the experiment in this paper. Another reason is that these particles would remain in the fractures. At this point, the particles act as proppants and the fractures cannot be closed completely. In the real stratum, some powdery particles may be carried away by the fracturing fluid, but the larger particles still stay in the fractures. In a word, those residues act as proppants. Hence, the fracture cannot be completely closed even if there is no added proppants in the fractures.

4.2.2. Equivalent Width of Fractures. The above discussed the reason why self-supporting fractures were still permeable.

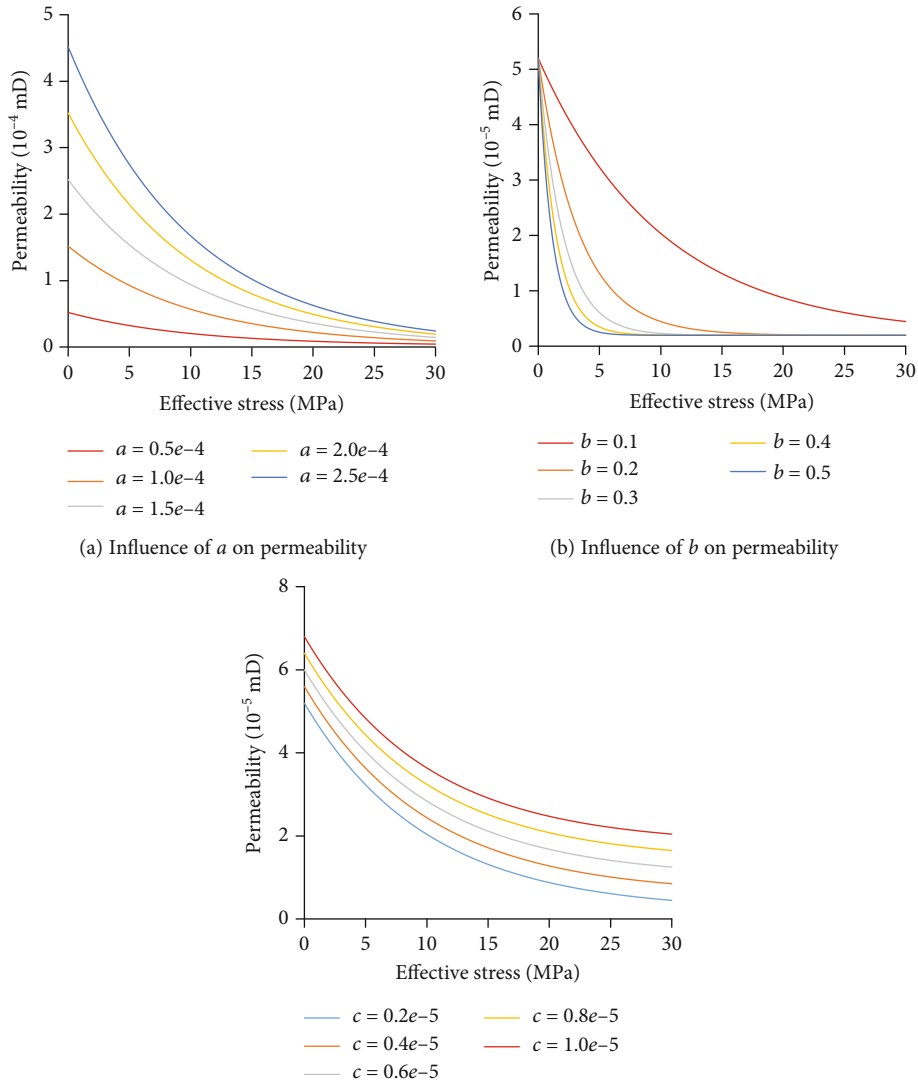

(a) Influence of a on permeability

(b) Influence of b on permeability

(c) Influence of c on permeability

Figure 10: The parameter analysis for the improved exponential model.

(a) (b)

Figure 11: Fracture surfaces and flaking particles.

The essential reason is a nonclosed fracture. The fracture is difficult to describe because of its roughness. In order to describe the self-supporting fractures, the equivalent fracture width is proposed to evaluate the fracture width in this study. Referring to Figure 2(b), the fracture surfaces are assumed as smooth surfaces in the middle of the core. Then, the permeability of fractured shale depends on the equivalent width of fracture. The equivalent width of fracture describes the permeability change with effective stress. According to Darcy's law and Reynold's equation for laminar flow between parallel surfaces, the equivalent width of fracture can be calculated.

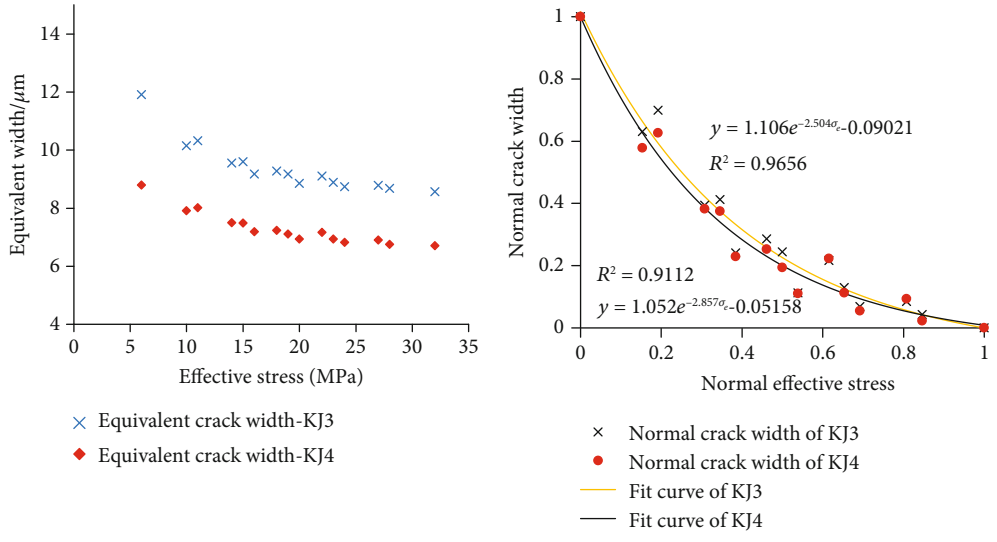

(a) Equivalent fracture width

(b) Normalization results

Figure 12: Relationship between equivalent width of fracture and effective stress.

By Darcy's law, the flow through the matrix can be expressed as

$$q_m = \frac{k_m A \Delta p}{\mu L}. \tag{9}$$

The flow through the fracture can be expressed as

$$q_f = \frac{k_f A \Delta p}{\mu L}. \tag{10}$$

The total flow is the sum of the flow in matrix and fracture

$$q_t = q_m + q_f. \tag{11}$$

By Darcy's law, the flow rate of the entire sample is

$$q_t = \frac{k_t A \Delta p}{\mu L} \tag{12}$$

Available from Equation (11),

$$q_f = q_t - q_m = q_m = \frac{(k_t - k_m) A \Delta p}{\mu L}. \tag{13}$$

In sum,

$$k_f = k_t - k_m. \tag{14}$$

Assuming that the fracture surfaces are a set of smooth planes and the fluid is laminar in the fracture, Reynold's equation for the parallel plate flow can be expressed as

$$q_f = \frac{e^3 \Delta p}{12 \mu L} * 2r. \tag{15}$$

Available from Equation (12) to Equation (15)

$$k_t - k_m = -\frac{\left(q_f + q_m - q_m\right)\mu L}{A \Delta p} = \frac{\left(\left(e^3 \Delta p / 12 \mu L\right) \cdot 2r\right)\mu L}{A \Delta p} = \frac{r e^3}{6A}. \tag{16}$$

The equivalent width of fracture is

$$e = \sqrt[3]{\frac{6A(k_t - k_m)}{r}}. \tag{17}$$

$$A = \pi r^2. \tag{18}$$

Substituting Equation (18) into Equation (17), the equivalent width can be simplified to

$$e = \sqrt[3]{6\pi r (k_t - k_m)}. \tag{19}$$

In the condition where the fracture is not closed, the pore pressure and confining pressure affect the width of the fracture. Figure 12(a) shows the variation of the equivalent fracture width with effective stress. As the figure shows, the equivalent width of fracture reduces as the effective stress rises. The equivalent width of fracture ranges from 6 to 12 μm. This value is small, but it has a great influence on the permeability of the fractured shale core. The experimental results shows that the artificial fractures effectively raise the permeability of the fractured sample. The core permeability is very sensitive to change in the fracture width. Because of the difference in rock samples, there is a certain difference in the equivalent fracture width in Figure 12(a). Then, what is the relationship between the fracture width and the effective stress?

The equivalent fracture width and the effective stress are normalized separately to investigate the relationship between them. The results after normalization are plotted

in Figure 12(b). The relationship between the equivalent width and the effective stress is attempted by the improved exponential relationship established above. The calculated fit goodness is greater than 0.9, so that the fitting effect is well. Therefore, the stress sensitivity of the fracture width can also be described by the improved exponential relationship. As a result, we can characterize the stress influence on the permeability of fractured shale according to stress sensitivity of the fracture width curve.

5. Conclusions

In this paper, the permeability of intact shale and fracture shale is measured by the transient pulse method. The relationship between shale permeability and stress was analyzed. The main conclusions are as follows:

(1) Comparing the results of fractured shale and intact shale, the fracture can greatly increase the permeability of the test rock sample. In this experiment, the permeability of the sample was increased by five orders of magnitude by the fractures

(2) The permeability of intact shale under low pore pressure and high pore pressure is measured. The results show that the variation of permeability with pore pressure shows different results under two different conditions. Under the condition of low pore pressure, the slippage effect in the matrix is significant, so the slippage effect is a key factor affecting the permeability change, and the permeability decreases with the increase of pore pressure. Under the condition of high pore pressure, the deformation of the matrix is the main factor affecting the change of permeability. At this time, the permeability increases with the increase of pore pressure. This result also indicates that the change in permeability is the result of the combined effect of slippage effect and matrix deformation

(3) The exponential function was improved in this paper. The improved exponential function can better fit the relationship between shale matrix permeability and effective stress for high pore pressure. It has a higher fitting accuracy compared with the traditional relationship. There are three advantages of the new model compared with the traditional model: better fitting accuracy, better mathematical form, and reflection of the overall error

(4) The fractures in fractured shale samples cannot be closed completely even when the confining pressure is bigger than the pore pressure. The fracture is still the main flow channel of the gas, and the permeability of fractured shale is still much larger than the matrix. It means that the permeability of reservoir would increase after fracturing. There are two explanations for this. One reason is that the fracture surfaces are rough. The displacement of the surfaces under shear stress causes the unclosed fractures. Another reason is the peeling of surface particles. The void forms after particle peeling. In addition, the exfoliated particles can act as a proppant to hinder the fracture closure

(5) Aiming at the problem that the fracture width is difficult to describe due to the roughness of the fracture surfaces, this paper proposes the concept of equivalent fracture width. The change in permeability can be characterized by the equivalent fracture width. The fitting results show that the relationship between the equivalent fracture width and the effective stress also satisfies the improved exponential relationship proposed in this paper

(6) The improved exponential relationship proposed in this paper is established under the condition of high pore pressure, only considering the relationship between permeability and effective stress and ignoring the slippage effect. Therefore, the improved exponential relationship in this paper is only applicable to high pore pressure conditions. In future research, different pore pressures should be combined to establish a permeability characterization equation that comprehensively considers the combined effect of slippage effect and matrix deformation

Data Availability

The data used to support the findings of this study are included within the article.

Conflicts of Interest

The authors declare that there is no conflict of interest regarding the publication of this article.

References

[1] S. C. Maxwell, T. I. Urbancic, N. Steinsberger, and R. Zinno, *Microseismic imaging of hydraulic fracture complexity in the Barnett Shale*, Society of Petroleum Engineers, San Antonio, Texas, 2002.

[2] G. Feng, X. Wang, M. Wang, and y. Kang, "Experimental investigation of thermal cycling effect on fracture characteristics of granite in a geothermal-energy reservoir," *Engineering Fracture Mechanics*, vol. 235, article 107180, pp. 1–16, 2020.

[3] W. Shen, X. Li, X. Lu, W. Guo, S. Zhou, and Y. Wan, "Experimental study and isotherm models of water vapor adsorption in shale rocks," *Journal of Natural Gas Science and Engineering.*, vol. 52, pp. 484–491, 2018.

[4] W. Shen, F. Song, X. Hu, G. Zhu, and W. Zhu, "Experimental study on flow characteristics of gas transport in micro- and nanoscale pores," *Scientific Reports*, vol. 9, no. 1, p. 10196, 2019.

[5] D. Yang, W. Wang, W. Chen, S. Wang, and X. Wang, "Experimental investigation on the coupled effect of effective stress and gas slippage on the permeability of shale," *Scientific Reports*, vol. 7, 2017.

[6] D. Ren, D. Zhou, D. Liu, F. Dong, S. Ma, and H. Huang, "Formation mechanism of the Upper Triassic Yanchang

Formation tight sandstone reservoir in Ordos Basin—Take Chang 6 reservoir in Jiyuan oil field as an example," *Journal of Petroleum Science and Engineering*, vol. 178, pp. 497–505, 2019.

[7] J. T. Chen, J. H. Zhao, S. C. Zhang, Y. Zhang, F. Yang, and M. Li, "An experimental and analytical research on the evolution of mining cracks in deep floor rock mass," *Pure and Applied Geophysics*, 2020.

[8] J. Wang, Y. Zhang, Z. Qin, S. G. Song, and P. Lin, "Analysis method of water inrush for tunnels with damaged water-resisting rock mass based on finite element method-smooth particle hydrodynamics coupling," *Computers and Geotechnics*, vol. 126, article 103725, 2020.

[9] K. Wu, Z. Chen, X. Li, C. Guo, and M. Wei, "A model for multiple transport mechanisms through nanopores of shale gas reservoirs with real gas effect–adsorption-mechanic coupling," *International Journal of Heat and Mass Transfer.*, vol. 93, pp. 408–426, 2016.

[10] G. Sheng, F. Javadpour, and Y. Su, "Effect of microscale compressibility on apparent porosity and permeability in shale gas reservoirs," *International Journal of Heat and Mass Transfer.*, vol. 120, pp. 56–65, 2018.

[11] D. Yang, W. Wang, and K. Li, "Experimental investigation on the stress sensitivity of permeability in naturally fractured shale," *Environmental Earth Sciences*, vol. 78, no. 2, 2019.

[12] J. J. Dong, J. Y. Hsu, W. J. Wu et al., "Stress-dependence of the permeability and porosity of sandstone and shale from TCDP hole-A," *International Journal of Rock Mechanics and Mining Sciences*, vol. 7, pp. 1141–1157, 2010.

[13] Y. Shi and C. Wang, "Pore pressure generation in sedimentary basins: overloading versus aquathermal," *Journal of Geophysical Research: Solid Earth*, vol. 91, no. B2, pp. 2153–2162, 1986.

[14] C. A. Morrow, L. Q. Shi, and J. D. Byerlee, "Permeability of fault gouge under confining pressure and shear stress," *Journal of Geophysical Research: Solid Earth*, vol. 89, no. B5, pp. 3193–3200, 1984.

[15] F. O. Jones Jr., "A laboratory study of the effects of confining pressure on fracture flow and storage capacity in carbonate rocks," *Journal of Petroleum Technology*, vol. 27, no. 1, pp. 21–27, 2013.

[16] J. B. Walsh, "Effect of pore pressure and confining pressure on fracture permeability," *International Journal of Rock Mechanics and Mining Sciences & Geomechanics Abstracts*, vol. 18, no. 5, pp. 429–435, 1981.

[17] R. Zhang, Z. Ning, F. Yang, X. Wang, H. Zhao, and Q. Wang, "Impacts of nanopore structure and elastic properties on stress-dependent permeability of gas shales," *Journal of Natural Gas Science and Engineering*, vol. 26, pp. 1663–1672, 2015.

[18] A. Ghanizadeh, M. Gasparik, A. Amann-Hildenbrand, Y. Gensterblum, and B. M. Krooss, "Experimental study of fluid transport processes in the matrix system of the European organic-rich shales: I. Scandinavian Alum Shale," *Marine and Petroleum Geology*, vol. 51, pp. 79–99, 2014.

[19] G. Cui, J. Liu, M. Wei, R. Shi, and D. Elsworth, "Why shale permeability changes under variable effective stresses: new insights," *Fuel*, vol. 213, pp. 55–71, 2018.

[20] M. Gutierrez, D. Katsuki, and A. Tutuncu, "Determination of the continuous stress-dependent permeability, compressibility and poroelasticity of shale," *Marine and Petroleum Geology*, vol. 68, pp. 614–628, 2015.

[21] Y. Wu, Z. Pan, D. Zhang, D. I. Down, Z. Lu, and L. D. Connell, "Experimental study of permeability behaviour for proppant supported coal fracture," *Journal of Natural Gas Science and Engineering*, vol. 51, pp. 18–26, 2018.

[22] Y. Tan, Z. Pan, J. Liu, Y. Wu, A. Haque, and L. D. Connell, "Experimental study of permeability and its anisotropy for shale fracture supported with proppant," *Journal of Natural Gas Science and Engineering*, vol. 44, pp. 250–264, 2017.

[23] Q. Yin, R. Liu, H. Jing, H. Su, L. Yu, and L. He, "Experimental study of nonlinear flow behaviors through fractured rock samples after high-temperature exposure," *Rock Mechanics and Rock Engineering*, vol. 52, no. 9, pp. 2963–2983, 2019.

[24] K. Su, Y. Sanz Perl, A. Onaisi, H. Pourpark, and S. Vidal-Gilbert, *Experimental study of hydromechanical behavior of fracture of Vaca Muerta Gas Shale*, American Rock Mechanics Association, San Francisco, California, USA, 2017.

[25] T. Zhou, S. Zhang, Y. Feng, Y. Shuai, Y. Zou, and N. Li, "Experimental study of permeability characteristics for the cemented natural fractures of the shale gas formation," *Journal of Natural Gas Science and Engineering.*, vol. 29, pp. 345–354, 2016.

[26] Y. Ma, Z. Pan, N. Zhong et al., "Experimental study of anisotropic gas permeability and its relationship with fracture structure of Longmaxi Shales, Sichuan Basin, China," *Fuel*, vol. 180, pp. 106–115, 2016.

[27] J. Zhou, L. Zhang, X. Li, and Z. Pan, "Experimental and modeling study of the stress-dependent permeability of a single fracture in shale under high effective stress," *Fuel*, vol. 257, 2019.

[28] Q. Yin, H. Jing, G. Ma, H. Su, and R. Liu, "Investigating the roles of included angle and loading condition on the critical hydraulic gradient of real rock fracture networks," *Rock Mechanics and Rock Engineering*, vol. 51, no. 10, pp. 3167–3177, 2018.

[29] C. Dong, Z. Pan, and Y. Zhihui, "Dependence of gas shale fracture permeability on effective stress and reservoir pressure: model match and insights," *Fuel*, vol. 139, pp. 383–392, 2015.

[30] Z. Gu, R. Liang, J. Su et al., "Impacts of pore-throat system on fractal characterization of tight sandstones," *Geofluids*, vol. 2020, Article ID 4941501, 2020.

[31] F. Ren, C. Zhu, and M. He, "Moment tensor analysis of acoustic emissions for cracking mechanisms during schist strain burst," *Rock Mechanics and Rock Engineering*, vol. 53, no. 1, pp. 153–170, 2020.

[32] C. E. Neuzil, C. Cooley, S. E. Silliman, J. D. Bredehoeft, and P. A. Hsieh, "A transient laboratory method for determining the hydraulic properties of 'tight' rocks—II. Application," *International Journal of Rock Mechanics and Mining Sciences & Geomechanics Abstracts*, vol. 18, no. 3, pp. 253–258, 1981.

[33] P. A. Hsieh, J. V. Tracy, C. E. Neuzil, J. D. Bredehoeft, and S. E. Silliman, "A transient laboratory method for determining the hydraulic properties of 'tight' rocks—I. Theory," *International Journal of Rock Mechanics and Mining Sciences & Geomechanics Abstracts*, vol. 18, no. 3, pp. 245–252, 1981.

[34] S. C. Jones, "A technique for faster pulse-decay permeability measurements in tight rocks," *SPE Formation Evaluation*, vol. 12, no. 1, pp. 19–26, 2013.

[35] C. Qian, G. Yanjie, and F. Tailiang, "The effect of pressure variation on gas permeability in fractured tight sandstone reservoir," *Science Technology and Engineering*, vol. 18, no. 26, pp. 60–67, 2018.

[36] Ø. Gutierrez, "Stress-dependent permeability of a demineralised fracture in shale," *Marine and Petroleum Geology*, vol. 17, no. 8, pp. 895–907, 2000.

[37] X. G. Duan, W. G. An, Z. M. Hu, S. S. Gao, L. Y. Ye, and J. Chang, "Experimental study on fracture stress sensitivity of Silurian Longmaxi shale formation, Sichuan Basin," *Natural Gas Geoscience*, vol. 28, no. 9, pp. 1416–1424, 2017.

[38] Q. Yin, G. Ma, H. Jing et al., "Hydraulic properties of 3d rough-walled fractures during shearing: an experimental study," *Journal of Hydrology*, vol. 555, pp. 169–184, 2017.